THE OFFICIAL MAGAZINE OF THE OCEANOGRAPHY SOCIETY

Oceanography

CITATION

Pun, I.F., Y.-T. Chang, I.-I. Lin, T.Y. Tang, and R.-C. Lien. 2011. Typhoon-ocean interaction in the western North Pacific: Part 2. *Oceanography* 24(4):32–41, http://dx.doi.org/10.5670/oceanog.2011.92.

DOI

http://dx.doi.org/10.5670/oceanog.2011.92

COPYRIGHT

This article has been published in *Oceanography*, Volume 24, Number 4, a quarterly journal of The Oceanography Society. Copyright 2011 by The Oceanography Society. All rights reserved.

USAGE

Permission is granted to copy this article for use in teaching and research. Republication, systematic reproduction, or collective redistribution of any portion of this article by photocopy machine, reposting, or other means is permitted only with the approval of The Oceanography Society. Send all correspondence to: info@tos.org or The Oceanography Society, PO Box 1931, Rockville, MD 20849-1931, USA.

DOWNLOADED FROM HTTP://WWW.TOS.ORG/OCEANOGRAPHY

Typhoon-Ocean Interaction in the Western North Pacific

Part 2

BY IAMFEI PUN, YA-TING CHANG, I.-I. LIN, TSWEN YUNG TANG, AND REN-CHIEH LIEN

Super Typhoon Maemi on September 10, 2003 (roughly a Category 5 hurricane on the Saffir-Simpson Hurricane Scale). Note Taiwan on the far left of the image. *Photo courtesy of Jacques Descloitres, MODIS Rapid Response Team, NASA/GSFC*

ABSTRACT. During summer 2010, the Taiwan National Science Council and the US Office of Naval Research conducted a large typhoon-ocean field experiment named Impact of Typhoons on the Ocean in the Pacific (ITOP). The goals were to investigate the highly complex physical processes associated with typhoon-ocean interactions. This article highlights the Taiwanese efforts during the ITOP experiments, including work on operational satellite-derived upper-ocean thermal structure and in situ observations from moorings. A brief review of typhoon-ocean interaction research in Taiwan is also provided.

INTRODUCTION

The term typhoon specifically refers to a tropical cyclone over the western North Pacific Ocean. According to the Saffir-Simpson Tropical Cyclone Scale, typhoons can be classified into five categories by their 1-min maximum sustained wind speeds: Category 1: 33–42 m s^{-1}, Category 2: 43–48 m s^{-1}, Category 3: 49–58 m s^{-1}, Category 4: 59–69 m s^{-1}, and Category 5: $\geq$ 70 m s^{-1}. Climatologically, the western North Pacific contains the highest number of tropical cyclones annually, and their intensity is also greater with respect to other cyclone-rich basins (Webster et al., 2005; Lin et al., 2005, 2008, 2009b). Based on the best-track typhoon data between 1970 and 2008 from the US Joint Typhoon Warning Center (JTWC), the average number of typhoons occurring each year in this basin is 16.5, of which 6.3 (38%) are super typhoons (Categories 4 and 5). Figure 1a shows all the Category 5 typhoons that occurred from May to October during the years 1993–2005. Typhoon intensification occurs in the area that lies from 10°N to 26°N, 121°E to 170°E, where warm waters regularly exist (Holliday and Thompson, 1979; Lin et al., 2008, 2009b).

In fact, typhoon and ocean are a tightly coupled system and their interaction involves many complex physical processes, such as waves and exchanges of momentum and heat at the air-sea interface (Price, 1981; Emanuel, 1986, 1995, 1997; Shay et al., 2000; Lin et al., 2003a, 2005, 2008, 2009a,b, 2011; Black et al., 2007; D'Asaro et al., 2007; Goni et al., 2009). Typhoons form and spend most of their lifetimes over the ocean. Through air-sea heat fluxes, the ocean provides the necessary energy for typhoon intensification. However, as typhoons traverse the ocean, their strong cyclonic winds also affect the upper ocean, typically from the surface to depths of 100–200 m, generating turbulence, currents, and waves. More importantly, relatively deep, cold water is upwelled to the surface layer, causing well-known cyclone-induced sea surface temperature (SST) cooling (Price, 1981; Lin et al., 2003a,b; D'Asaro et al., 2007). As such, SST cooling is a primary negative feedback mechanism of cyclone intensification because cool surface waters can reduce and even cut off a typhoon's energy supply from the ocean (Emanuel, 1999; Cione and Uhlhorn, 2003; Lin et al., 2005, 2008, 2009a,b, 2011). Mesoscale oceanic features (e.g., eddies) modulate SST cooling and thus have considerable impact on typhoon intensity (Shay et al., 2000; Lin et al., 2005, 2008, 2009a,b;

Wu et al., 2007). For example, Typhoon Maemi (2003) intensified to super typhoon strength after passing a series of warm ocean features (see Figure 1b; intensification from a Category 1 to a Category 5 typhoon occurred from 1800 UTC on September 8 to 0000 UTC on September 10; Lin et al., 2005). In Figure 1b, note the two well-defined eddy-rich zones (i.e., the north and south eddy zones in which warm and cold eddies occur year-round).

Cold wakes left behind by typhoons can persist for weeks to a month (Lin et al., 2003a,b; Price et al., 2008). During this period, they continually affect atmosphere and ocean, and even subsequent typhoons (Emanuel, 2001; Lin et al., 2003a). In addition, strong typhoon winds cause upwelling of nutrients from the deeper ocean to the euphotic zone, leading to phytoplankton blooms (Lin et al., 2003b; Hung and Gong, 2011, in this issue).

Because it is extremely difficult to observe the interaction between typhoons and the ocean under severe typhoon conditions, knowledge of this complex coupled system is still very limited. Given the frequent occurrence of typhoons and abundant oceanic features, the western North Pacific is an ideal place to study this interaction. Thus, the Taiwan National Science Council (NSC) and the US Office of Naval Research (ONR) supported a large joint field experiment called Impact of Typhoons on the Ocean in the Pacific (ITOP) from August to October 2010. The objective of ITOP was to explore typhoon-ocean interactions in detail, especially the ocean's response to typhoons, and typhoons' intensity

changes, with the goal of improving typhoon intensity forecasting. This article highlights the Taiwanese efforts and preliminary results of ITOP, while D'Asaro et al. (2011, in this issue) summarize the contributions to ITOP made by US scientists. In addition, Taiwanese ITOP atmospheric observations of typhoons were gathered by the Dropsonde Observation for Typhoon Surveillance near the TAiwan Region (DOTSTAR; Wu et al., 2005) team using the Taiwanese Astra aircraft. We also briefly review the typhoon-ocean research conducted in Taiwan in the last decade.

SATELLITE-DERIVED, NEAR-REAL-TIME, UPPER-OCEAN THERMAL STRUCTURE

Upper-ocean thermal structure (UOTS) plays a crucial role in typhoon intensification because typhoons interact not only with surface waters but also with the entire upper-ocean water column, generally in a depth range of 0–200 m (Leipper and Volgenau, 1972; Holliday and Thompson, 1979; Shay et al., 2000; Goni and Trianaes, 2003; Lin et al., 2005, 2008, 2009a,b; Goni et al., 2009). In a typical UOTS profile, temperature decreases with depth. UOTS is directly related to typhoon-induced SST cooling. If there is a thick subsurface warm-water layer (usually to the depth of the 26°C isotherm [$D26$], above which the water is regarded as warm), little deep cold water will be entrained into the mixed layer by the storm, and SST cooling will be suppressed. By contrast, if a typhoon travels over a shallow $D26$ ocean, deep cold water can easily be entrained into the surface layer, resulting in considerable SST cooling that can potentially obstruct typhoon intensification.

Traditionally, the information on UOTS could only be obtained by in situ means, such as ships, moorings, and floats. Because it is extremely difficult to collect such observations under typhoon conditions, lack of subsurface information posed a fundamental obstacle to further understanding the mechanisms of typhoon-ocean interaction. Therefore, ITOP aimed to extensively observe the evolution of UOTS during typhoons by using an array of advanced instruments, such as Airborne Expendable
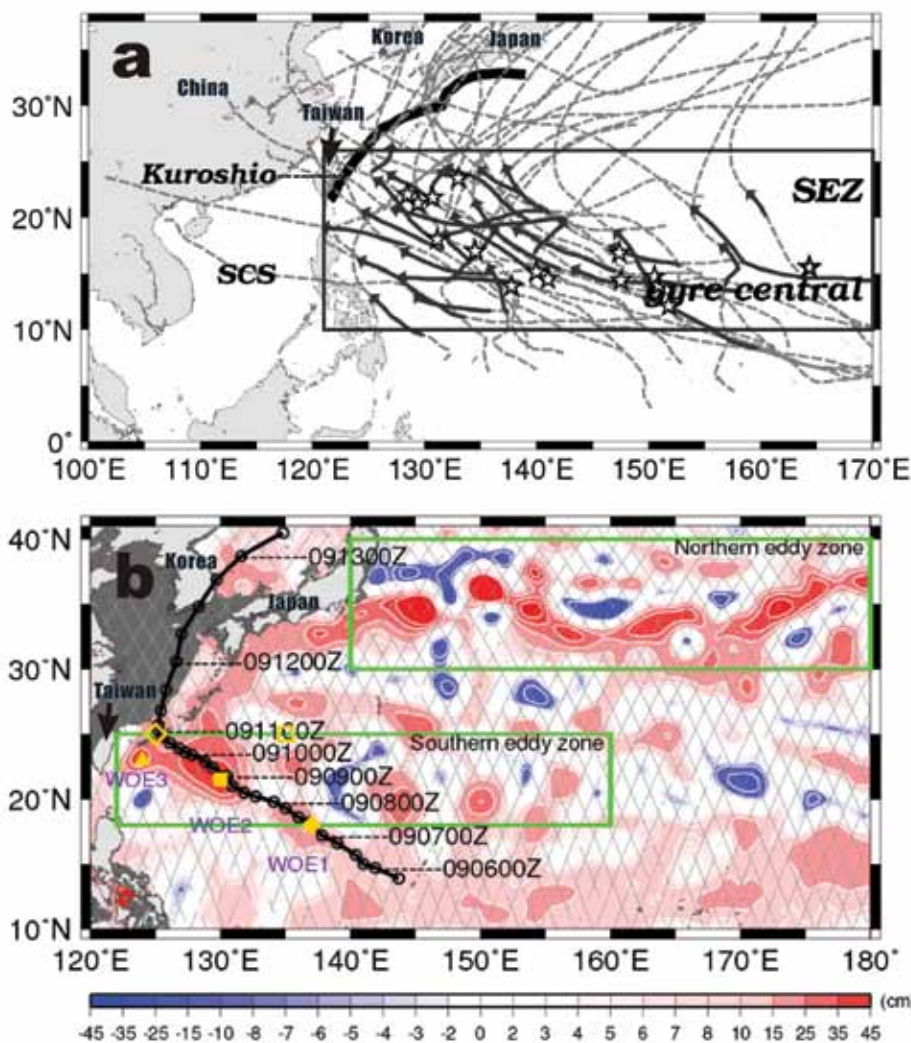

Figure 1. (a) Category 5 typhoons that occurred from May to October between 1993 and 2005 from the US Joint Typhoon Warning Center. Dashed curves depict the full typhoon tracks, and solid curves with arrows indicate track segments where the typhoons intensified from Category 1 to Category 5 (after Lin et al., 2008). The black box encompasses the typhoon intensification area. SCS = South China Sea. SEZ = Southern Eddy Zone. (b) Sea surface height anomaly composite of TOPEX/Poseidon and Jason-1 altimeter data between August 27 and September 5, 2003. Light gray grid lines trace the ground tracks of the altimeters. The heavy black line depicts the track of Super Typhoon Maemi (2003), with date stamps to the right of the track. Maemi's main intensification period is from 1800 UTC September 8 (the last Category 1 point) to 0000 UTC September 10 (Category 5). The solid diamond, solid square, and solid triangle mark the locations of warm ocean eddies WOE 1, WOE 2, and WOE 3, respectively. The open diamond and open square show the locations of peripheral and background eddies, respectively. The two green boxes outline the Northern Eddy Zone and the Southern Eddy Zone. *After Lin et al. (2005)*

Bathythermographs (AXBTs), EM-APEX floats (D'Asaro et al., 2007), and Seagliders. In addition, advances in satellite altimetry now make it possible to estimate UOTS using satellite-measured sea surface height anomalies (SSHA); variations in subsurface temperature are physically related to variations in sea surface height. Figure 1b shows a map of satellite SSHA. Positive (negative) SSHA features generally mean that subsurface temperature is warmer (colder) and D26 is deeper (shallower) than climatology.

Here, the two-layer reduced gravity scheme proposed by Goni et al. (1996) and Shay et al. (2000) is adopted to estimate UOTS in the western North Pacific from the SSHA data (Pun et al., 2007). The Figure 2a schematic shows the calculated satellite-derived UOTS. It consists of four elements that include the 20°C isotherm depth ($D20$), $D26$, SST, and mixed layer depth (MLD). First, $D20$ is estimated from SSHA by the two-layer scheme:

$$D20(x, y, t) = \overline{D20}(x, y) + \frac{\rho_2(x, y)}{\rho_2(x, y) - \rho_1(x, y)} \eta'(x, y, t), \quad (1)$$

where $\overline{D20}$ is the climatological $D20$ based on the World Ocean Atlas 2001 (http://www.nodc.noaa.gov/OC5/WOA01/woa01dat.html) temperature analysis; ρ_1 and ρ_2 are the densities of the upper (surface to $D20$) and lower ($D20$ to the ocean bottom) layers, respectively; and η_1 is SSHA. The SSHA data used are the real-time (one-day delay) 1/4° gridded and merged product from AVISO (Archiving, Validation and Interpretation of Satellite Oceanographic data). In this data set, SSHA from all available satellite altimeters are combined in order to maximize the spatial resolution and to enhance the accuracy of SSHA maps. Presently, four altimeter missions (i.e., ERS-2 [1995], Envisat [2002], Jason-1 [2001], and Jason-2 [2008]) are functional, providing high-quality SSHA observations. Second, $D26$ is computed from derived $D20$ by using a climatological ratio between $D26$ and $D20$. Next, SST is obtained from the Remote Sensing System (Wentz et al., 2000), which combines SST from the cloud-penetrating Tropical Rainfall Measuring Mission (TRMM)/Microwave Imager (TMI) and Advanced Microwave Sounding Radiometer for the Earth Observing System (AMSR-E). Lastly, in order to derive more realistic temperature profiles, the climatological monthly MLD from the US Naval Research Laboratory (NRL) is used to describe a mixed layer in which temperature is equal to SST. Thus, a first-order estimation of UOTS can be obtained (Figure 3c,d).

During the ITOP Intensive Operational Period (IOP; August–October 2010), we used this method to produce the western North Pacific's UOTS in near-real time for identification of ocean features to be targeted for deployment of in situ instruments, and for planning strategic observations. During the operation, a set of horizontal maps

IamFei Pun *is PhD Candidate, Department of Atmospheric Sciences, National Taiwan University, Taipei, Taiwan.* **Ya-Ting Chang** *is PhD Candidate, Institute of Oceanography, National Taiwan University, Taipei, Taiwan.* **I.-I. Lin** *(iilin@as.ntu.edu.tw) is Professor, Department of Atmospheric Sciences, National Taiwan University, Taipei, Taiwan.* **Tswen Yung Tang** *is Professor, Institute of Oceanography, National Taiwan University, Taipei, Taiwan.* **Ren-Chieh Lien** *is Principal Oceanographer and Affiliate Professor, Oceanography, Applied Physics Laboratory, University of Washington, Seattle, WA, USA.*
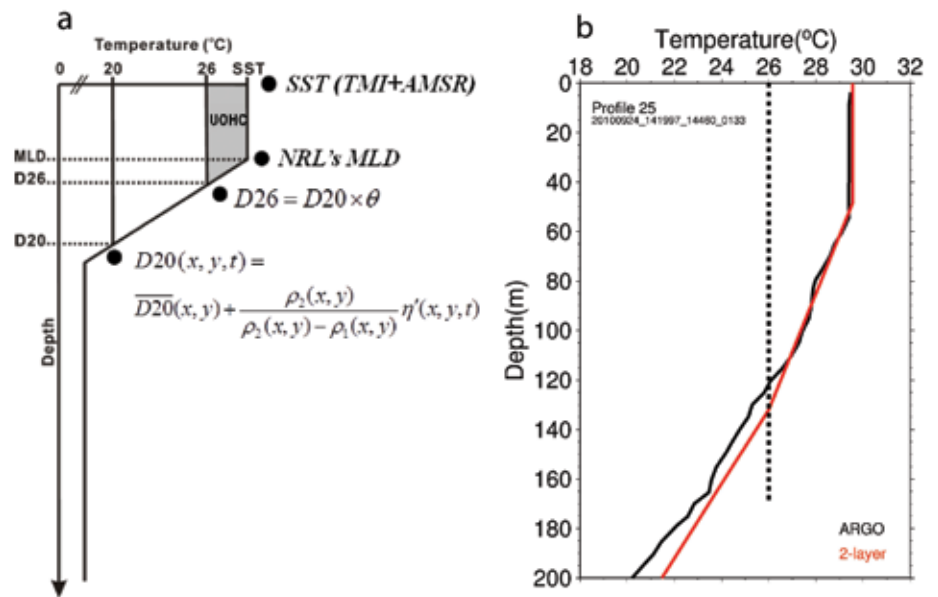
Figure 2. (a) This schematic of satellite-derived upper-ocean thermal structure consists of sea surface temperature (SST), mixed-layer depth (MLD), D26 (the depth of the 26°C isotherm, above which the water is regarded as warm), and D20 (the depth of the 20°C isotherm). (b) Comparison of Argo float (black) and satellite-derived (red) temperature profiles. See Figure 3 for the profile's location (Profile 25).

of SST, SSHA, $D26$, upper-ocean heat content (UOHC; i.e., the heat content in excess of 26°C as integrated from the surface to $D26$; Leipper and Volgenau, 1972), and $T_{\overline{100}}$ (average temperature of the upper 100 m of the water column;

Price, 2009) were generated on a daily basis. For example, Figure 3a–e shows the maps of SST, SSHA, $D26$, UOHC, and $T_{\overline{100}}$ on September 24, 2010, respectively. On these daily maps, all real-time accessible in situ data (including those

observed by ITOP) are superimposed to provide additional information and quick comparisons with the estimated field. Such additional information includes all Argo floats within a two-day period (color-coded triangles), moorings
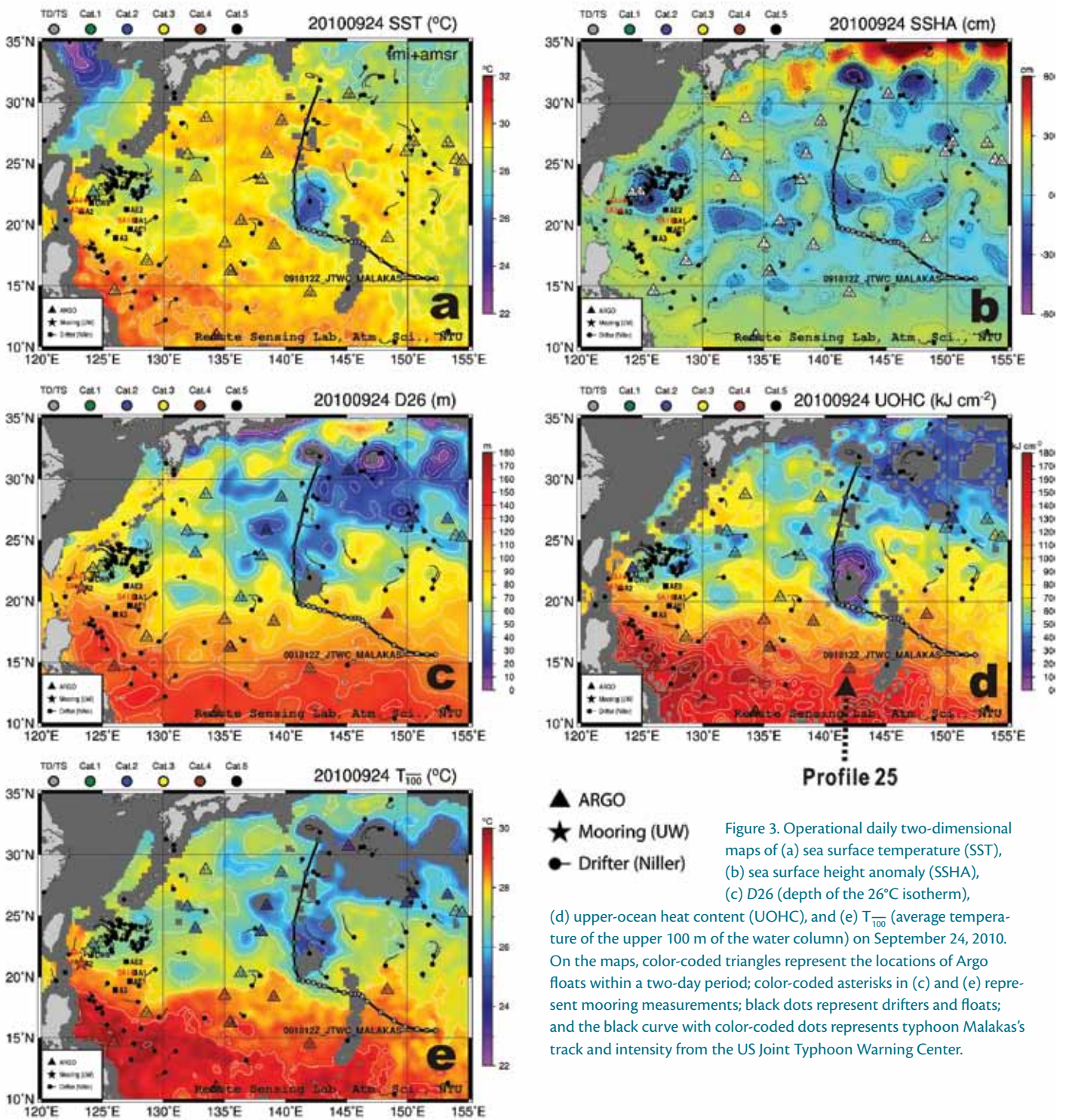

▲ ARGO
★ Mooring (UW)
●— Drifter (Niller)

Figure 3. Operational daily two-dimensional maps of (a) sea surface temperature (SST), (b) sea surface height anomaly (SSHA), (c) $D26$ (depth of the 26°C isotherm), (d) upper-ocean heat content (UOHC), and (e) $T_{\overline{100}}$ (average temperature of the upper 100 m of the water column) on September 24, 2010. On the maps, color-coded triangles represent the locations of Argo floats within a two-day period; color-coded asterisks in (c) and (e) represent mooring measurements; black dots represent drifters and floats; and the black curve with color-coded dots represents typhoon Malakas's track and intensity from the US Joint Typhoon Warning Center.

(color-coded asterisks), drifters (black dots), air-deployed instruments, and the typhoon tracks (observed and predicted), if available.

From the example maps in Figure 3, satellite SST (Figure 3a) and estimated $D26$, UOHC, and $T_{\overline{100}}$ (Figure 3c–e) show good agreement with the Argo and mooring observations. The subsurface parameters (i.e., $D26$, UOHC, and $T_{\overline{100}}$) give much more information than SST alone. Generally, subsurface temperature is higher in the south and lower in the north and varies associated with mesoscale features. For example, $D26$ at low latitudes (10–15°N) is as high as 160 m, while it decreases to 20–30 m at higher latitudes (30–35°N; Figure 3c). In contrast, SST is rather homogeneous from about 29–30°C. It is noteworthy that a cold wake located around 20°N, 142°E to the right of Typhoon Malakas's passage can be clearly seen (blue patch in Figure 3a). UOHC in this cold wake became very low (~ 10 KJ cm⁻²), even zero (Figure 3d). Note that the dense observations east of Taiwan around 23°N, 127°E are from the instruments deployed by the C-130 aircraft during ITOP from September 12–21, 2010 to capture Typhoon Fanapi. In order to provide a real-time comparison between in situ and derived temperature profiles, all Argo profiles on the daily maps are plotted individually with the satellite-derived profiles. Figure 2b compares profiles from Argo and the two-layer estimation. The estimated profile (red curve) is in good agreement with

the Argo profile (black curve), showing that, although it only contains four depths, the two-layer estimated UOTS is suitable for use with reasonable accuracy. In addition to the plan-view maps, values of the above five parameters as well as UOTS along the typhoon track were provided operationally during the ITOP IOP (not shown).

These various daily products were used to provide a synoptic picture of the ocean in the western North Pacific, and were useful in planning the daily flight and the cruises during the IOP, especially when we were attempting

to observe specific and scientifically interesting features (e.g., eddies, oceanic fronts). Meanwhile, several sophisticated atmosphere-ocean coupled models were operational during the experiment, but more often than not, these models generated diverse results. In this circumstance, satellite-derived UOTS was used to verify model performance.

Figure 4 compares $T_{\overline{100}}$ from National Taiwan University (NTU)'s satellite estimation and NRL's East Asian Seas Ocean Nowcast/Forecast System (EASNFS) with observations from Argo (blue triangles) and AXBTs (red triangles) on
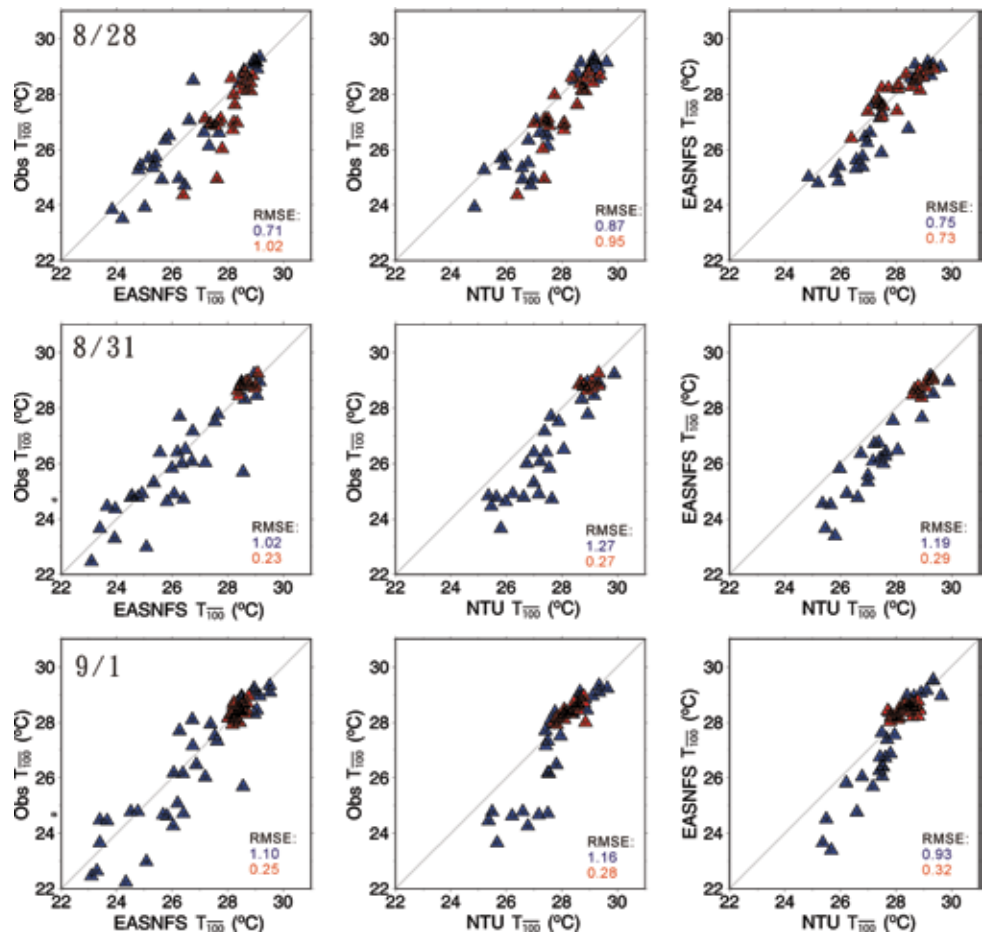

Figure 4. Intercomparison of $T_{\overline{100}}$ from National Taiwan University (NTU)'s satellite estimation, the US Naval Research Laboratory's East Asian Seas Ocean Nowcast/Forecast System (EASNFS), Argo floats (blue triangles), and airborne expendable bathythermographs (AXBTs; red triangles) on August 28, August 31, and September 1, 2010. The left column compares EASNFS and Argo and AXBT observations; the middle column compares satellite-derived observations and in situ data; the right column compares estimations from EASNFS and satellite data. The RMS errors are shown in each plot.

August 28, August 31, and September 1, 2010. Both the EASNFS model and the satellite estimation are generally consistent with the Argo and AXBT observations (the left and middle columns in Figure 4). The data show that $T_{\overline{100}}$ from Argo floats has a larger range of variation than that from the AXBTs. Especially on August 31 and September 1, 2010, the former ranges from 22–30°C, while the latter is constrained around 29°C. This can be explained by the location of the instruments—the AXBTs were only deployed in the warm pool region (i.e., south of 20°N) on those two days, while the Argo floats were spread over the entire basin (Figure 3). Compared with Argo data, the averaged RMS error of $T_{\overline{100}}$ in the EASNFS full ocean model is 0.94°C, while the error in the satellite estimation (i.e., from the two-layer method) is slightly higher (1.1°C). Compared to AXBTs, estimates from EASNFS and the two-layer method both have an error of 0.5°C. The averaged RMS difference between satellite-derived and EASNFS $T_{\overline{100}}$ is about 0.95°C (right column in Figure 4). These preliminary results show that the simple two-layer method is able to estimate the UOTS in the western North Pacific with reasonable accuracy, and it is even comparable to the sophisticated full ocean model. Efforts to improve the accuracy in satellite-derived UOTS are still ongoing.

IN SITU OBSERVATIONS FROM ITOP MOORINGS

The observations based on moored buoys are a result of collaboration among the Institute of Oceanography/ National Taiwan University, Taiwan Ocean Research Institute/National Applied Research Laboratory, and Applied Physical Laboratory/University

of Washington. Two different mooring designs were used for observing oceanic responses to typhoons. One is a surface mooring modified from an ATLAS (Autonomous Temperature Line Acquisition System) buoy that is equipped with meteorological sensors and subsurface temperature sensors. The second is a subsurface mooring equipped with an acoustic Doppler current profiler (ADCP) to monitor the upper-ocean currents. Meteorological parameters include air pressure, air temperature, relative humidity, wind speed, wind direction, and solar irradiance. All data were transmitted to shore via the Iridium satellite.

The pilot study began in August 2008 with one surface mooring deployed by Taiwan's R/V *Ocean Researcher 1*. The mooring successfully transmitted data and survived a typhoon, suggesting that its design was suitable for the ITOP experiment. In March 2009, the mooring was refurbished, and the US R/V *Kilo Moana* deployed two additional moorings with the same design. After those deployments, the US R/V *Roger Revelle* serviced the moorings every six months. Before ITOP began in August 2010, one additional surface mooring and three subsurface moorings were deployed.

The moorings were positioned along the most-frequent typhoon tracks off Taiwan. During the typhoon season of 2009, several typhoons, including Molave (Category 1), Morakot (Category 1), and Lupit (Category 5), passed by or crossed over one or more of these mooring stations. During 2009, the eye of Typhoon Lupit passed over one station and the eye wall passed over another mooring. Figure 5a shows Typhoon Lupit's track (from JTWC) and SST from

the three mooring stations embedded in the merged satellite SST at 1800 UTC on October 20, which was the closest time of approach of the eye of Typhoon Lupit to the station. The cold wake can be seen along Typhoon Lupit's track (blue colors in Figure 5a). Compared with the SST before the typhoon, a near 5°C SST drop was observed. In situ SSTs from the three stations were lower than satellite-observed SST because the satellite-merged SST was updated only daily. The time series of air pressure for mooring A1 (Figure 5b) recorded a lowest value of 942 hPa, even lower than what JTWC posted. While air pressure was dropping, the wind speed at that site (Figure 5d) increased to over 59 m s^{-1}. The air temperature (Figure 5c) slightly increased when the air pressure dropped quickly. At the same time, the SST changed gradually. Temperature did not decrease much until the typhoon moved away from the station. The upper-ocean temperature profile at mooring A1 (Figure 5e) varied in a similar way to SST observations. The temperature dropped dramatically—by 6°C—after the typhoon passed. The temperature profile oscillated at near-inertial frequency and recovered 10 days after the typhoon.

Station A3 recorded the lowest air pressure of 955 hPa (data not shown here), which is also lower than the value JTWC posted. The wind-speed time series showed a bell-shaped variation with the highest value of 46 m s^{-1}. Although the eye of the typhoon did not pass directly over this station, it also recorded a near 4°C SST drop, strong upwelling, and near-inertial responses in the upper ocean.

Although the ATLAS-like moorings were successfully deployed over the South China Sea (Chang et al., 2010),

the upper-ocean response beneath the typhoon's eye or eye wall had not been observed. More information will be obtained after further detailed analysis.

TYPHOON-OCEAN RESEARCH IN TAIWAN

Taiwan is located in a region where typhoons occur year-round (Figure 1). On average, three to four typhoons strike Taiwan annually and cause much damage. Although typhoon research has long been a focus of Taiwan's atmospheric scientists in the last decade, the oceanographic community in Taiwan began conducting extensive research on typhoon-ocean interaction because of the strong impact typhoons and the ocean have on each other. Here, we provide a brief review of recent typhoon-ocean research in Taiwan.

Using TMI SST and QuikSCAT surface wind vector data, Lin et al. (2003a) observed that moderate Category 2 Typhoon Kai-Tak (2000) left an intensive cold wake of 6–9°C in the South China Sea (SCS) southwest of Taiwan. This cold wake acted to stabilize the atmospheric boundary layer, causing the reduction of above-surface wind speed compared with wind speed outside the wake area. This observational result suggests that the impact of typhoons on the ocean can continually feed back to the atmosphere

as long as the cold wake remains.

In addition, Lin et al. (2003b) noted a strong phytoplankton bloom in Kai-Tak's wake. SeaWiFS images of chlorophyll a (Chl a) concentration showed that Chl a increased ~ 300% after Kai-Tak passed. Because this typhoon moved slowly, at about 0–1.4 m s^{-1}, it induced strong mixing and upwelling of cold water as well as nutrients from the deep ocean, resulting in the observed extreme cooling (~ 9°C) and the phytoplankton bloom (Lin et al., 2003b). This large increase in Chl a concentration accounted for 2–4% of the annual marine primary production in the South China Sea, indicating a strong biogeochemical response to typhoons. Similar cooling and phytoplankton blooms were observed after other typhoons, such as Nari (2001; Wu et al., 2008)

and Hai-Tang (2005; Chang et al., 2008; Zheng et al., 2008). The above satellite observations and numerical experiments are consistent with the in situ measurements recorded by Shiah et al. (2000), who observed that nutrient and Chl a concentrations increased after the passages of typhoons in the southern East China Sea (ECS). Recently, Lin (in press) found that the typhoon-induced phytoplankton blooms were relatively minor in the western North Pacific subtropical ocean compared with the marginal seas (i.e., SCS and ECS). Thus, we surmise that typhoons might play a critical role in the ocean's ecological and environmental systems because phytoplankton take up carbon dioxide and release oxygen. Note that during the ITOP cruises, in situ biogeochemical measurements were obtained
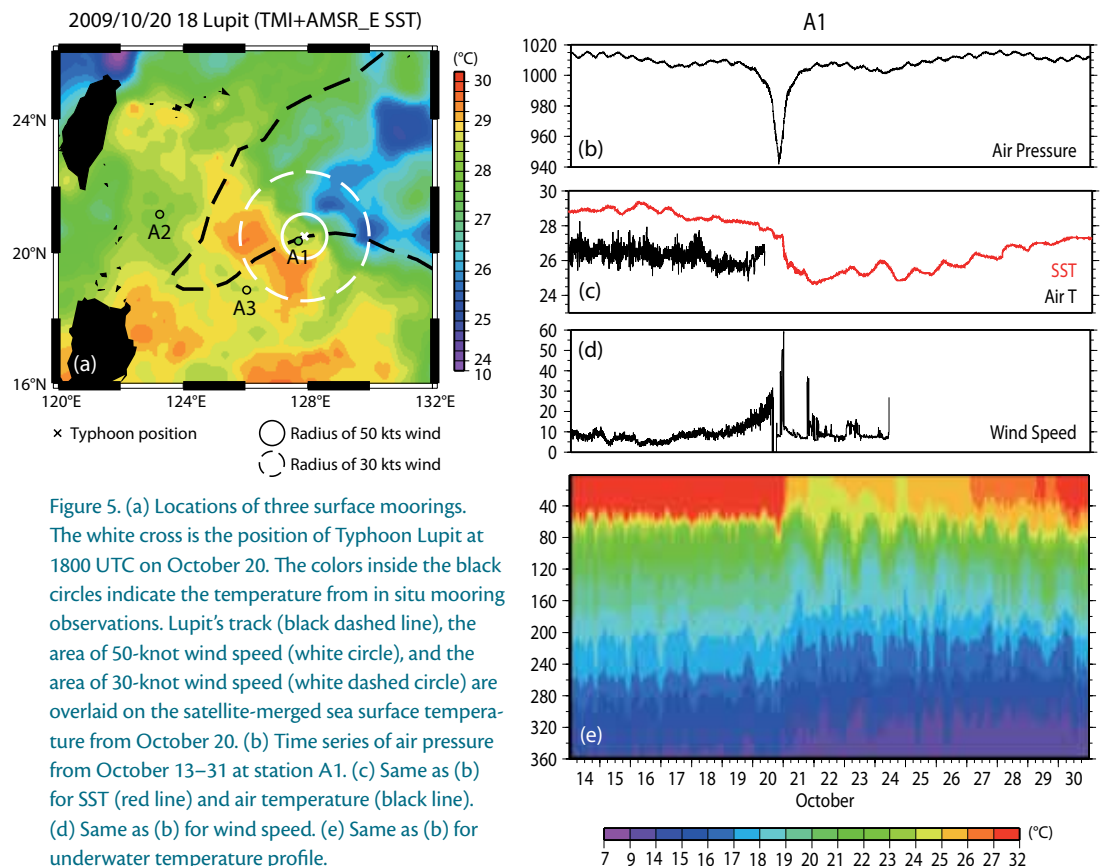

Figure 5. (a) Locations of three surface moorings. The white cross is the position of Typhoon Lupit at 1800 UTC on October 20. The colors inside the black circles indicate the temperature from in situ mooring observations. Lupit's track (black dashed line), the area of 50-knot wind speed (white circle), and the area of 30-knot wind speed (white dashed circle) are overlaid on the satellite-merged sea surface temperature from October 20. (b) Time series of air pressure from October 13–31 at station A1. (c) Same as (b) for SST (red line) and air temperature (black line). (d) Same as (b) for wind speed. (e) Same as (b) for underwater temperature profile.

to further explore such a response (Hung and Gong, 2011, in this issue).

Recent observations in the Atlantic show that a notable number of intense hurricanes, including Opal (1995; Shay et al., 2000) and Katrina (2005; Scharroo et al., 2005), rapidly intensified while they were passing over warm ocean eddies. Because there are abundant eddies in the western North Pacific (Figure 1), it is interesting to examine typhoon interaction with and response to these features. Finding that Super Typhoon Maemi (2003) became Category 5 when it passed over a warm ocean eddy (Figure 1b, 1800 UTC on September 8 to 0000 UTC on September 10), Lin et al. (2005) used multiple satellite observations and a series of numerical experiments to clarify the impact of an ocean eddy on typhoon intensity. They found that a warm eddy can increase typhoon intensity by one category because the warm eddy effectively suppresses the typhoon's SST cooling. Similarly, Pun et al. (2007) found that Super Typhoon Dianmu (2004) suddenly intensified as it traveled over a large warm ocean feature. Lin et al. (2008) discovered that nearly 30% of Category 5 typhoons intensified in the western North Pacific Ocean as a result of being influenced by warm ocean features. The influence of a warm eddy has also been observed in the Indian Ocean. Tropical Cyclone Nargis (2008) rapidly intensified after encountering a warm ocean feature just before landfall (Lin et al., 2009a). When Wu et al. (2007) used a typhoon-ocean coupled model to investigate the impact of a warm ocean eddy, the result showed that encountering a warm eddy can enhance energy fluxes and cause rapid intensification of a typhoon. In addition,

it was found that the warm Kuroshio current may also affect typhoon intensity (Lin et al., 2008; Wu et al., 2008). Wu et al. (2008) used observations and model simulation to show that typhoon intensity may increase as it crosses over the Kuroshio. Furthermore, Lin et al. (2011) suggested that the presence of warm ocean eddies contributed to Typhoon Morakot's (2009) extreme rainfall, which severely damaged southern Taiwan.

In addition to ocean features, the typhoon's translation speed is a critical factor in typhoon intensification. Lin et al. (2009b) found that it is possible for a strong typhoon to intensify over a shallow $D26$ if it moves fast enough because there is less SST cooling. However, a slow-moving storm needs a relatively thick $D26$ to restrain SST cooling because the affected depth in the ocean is much deeper.

Several modeling efforts were devoted to investigating the ocean response to typhoons (e.g., Tsai et al., 2008; Wu et al., 2008; Tseng et al., 2010; Chiang et al., 2011). Tsai et al. (2008) and Wu et al. (2008) studied the interaction between typhoons and the Kuroshio and concluded that typhoons may affect the current's path. Tseng et al. (2010) and Chiang et al. (2011) used a three-dimensional model to investigate the ocean's response to Typhoon Kai-Tak and found that upwelling associated with the typhoon's slow translation speed mainly caused intense cooling, whereas ocean mixing was a secondary mechanism.

FUTURE WORK

There are still many unresolved scientific issues associated with complex typhoon-ocean interaction processes, including

resolution of heat fluxes under high-wind conditions, which is one of the core issues in understanding the mechanism of typhoon intensification, and the evolution and recovery of the typhoon cold wake, which significantly influence both the atmosphere and the ocean. The valuable in situ measurements from ITOP will enable further exploration and understanding of such processes in this coupled system, resulting in improved forecasts of typhoon intensity.

REFERENCES

Black, P.G., E.A. D'Asaro, W.M. Drennan, J.R. French, P.P. Niiler, T.B. Sanford, E.J. Terrill, E.J. Walsh, and J.A. Zhang. 2007. Air-sea exchange in hurricanes: Synthesis of observations from the Coupled Boundary Layer Air-Sea Transfer Experiment. *Bulletin of the American Meteorological Society* 88:357–374, http://dx.doi.org/10.1175/BAMS-88-3-357.

Chang, Y., H.T. Liao, M.A. Lee, J.W. Chan, W.J. Shieh, K.T. Lee, G.H. Wang, and Y.C. Lan. 2008. Multisatellite observation on upwelling after the passage of Typhoon Hai-Tang in the southern East China Sea. *Geophysical Research Letters* 35, L03612, http://dx.doi.org/10.1029/2007GL032858.

Chang, Y.-T., T.Y. Tang, S.-Y. Chao, M.-H. Chang, D.S. Ko, Y.J. Yang, W.-D. Liang, and M.J. McPhaden. 2010. Mooring observations and numerical modeling of thermal structures in the South China Sea. *Journal of Geophysical Research* 115, C10022, http://dx.doi.org/10.1029/2010JC006293.

Chiang, T.-L., C.-R. Wu, and L.-Y. Oey. 2011. Typhoon Kai-Tak: An ocean's perfect storm. *Journal of Physical Oceanography* 41:221–233, http://dx.doi.org/10.1175/2010JPO4518.1.

Cione, J.J., and E.W. Uhlhorn. 2003. Sea surface temperature variability in hurricanes: Implications with respect to intensity change. *Monthly Weather Review* 131:1,783–1,796, http://dx.doi.org/10.1175/2562.1.

D'Asaro, E., P. Black, L. Centurioni, P. Harr, S. Jayne, I.-I. Lin, C. Lee, J. Morzel, R. Mrvaljevic, P.P. Niiler, and others. 2011. Typhoon-ocean interaction in the western North Pacific: Part 1. *Oceanography* 24(4):24–31, http://dx.doi.org/10.5670/oceanog.2011.91.

D'Asaro, E.A., T.B. Sanford, P.P. Niiler, and E.J. Terrill. 2007. Cold wake of Hurricane Frances. *Geophysical Research Letters* 34, L15609, http://dx.doi.org/10.1029/2007GL030160.

Emanuel, K.A. 1986. An air-sea interaction theory for tropical cyclones: Part I. Steady-state maintenance. *Journal of the Atmospheric Sciences* 42:1,062–1,071, http://dx.doi.org/10.1175/1520-0469(1986)043<0585:AASITF>2.0.CO;2.

Emanuel, K.A. 1995. Sensitivity of tropical cyclones to surface exchange coefficients and a revised steady-state model incorporating eye dynamics. *Journal of the Atmospheric Sciences* 52:3,969–3,976, http://dx.doi.org/10.1175/1520-0469(1995)052<3969:SOTCTS>2.0.CO;2.

Emanuel, K.A. 1997. Some aspects of hurricane inner-core dynamics and energetics. *Journal of the Atmospheric Sciences* 54:1,014–1,026, http://dx.doi.org/10.1175/1520-0469(1997)054<1014:SAOHIC>2.0.CO;2.

Emanuel, K.A. 1999. Thermodynamic control of hurricane intensity. *Nature* 401:665–669.

Emanuel, K.A. 2001. The contribution of tropical cyclones to meridional heat transported by the oceans. *Journal of Geophysical Research* 106(D14):14,771–14,781, http://dx.doi.org/10.1029/2000JD900641.

Goni, G., M. DeMaria, J. Knaff, C. Sampson, I. Ginis, F. Bringas, A. Mavume, C. Lauer, I.-I. Lin, M.M. Ali, and others. 2009. Applications of satellite-derived ocean measurements to tropical cyclone intensity forecasting. *Oceanography* 22(3):190–197, http://dx.doi.org/10.5670/oceanog.2009.78.

Goni, G.J., S. Kamholtz, S. Garzoli, and D.B. Olson. 1996. Dynamics of the Brazil–Malvinas confluence based upon inverted echo sounders and altimetry. *Journal of Geophysical Research* 101(7):16,273–16,289, http://dx.doi.org/10.1029/96JC01146.

Goni, G.J., and J.A. Trinanes. 2003. Ocean thermal structure monitoring could aid in the intensity forecast of tropical cyclones. *Eos, Transactions, American Geophysical Union* 84:573–580, http://dx.doi.org/10.1029/2003EO510001.

Holliday, C.R., and A.H. Thompson. 1979. Climatological characteristics of rapidly intensifying typhoons. *Monthly Weather Review* 107:1,022–1,034, http://dx.doi.org/10.1175/1520-0493(1979)107<1022:CCORIT>2.0.CO;2.

Hung, C.-C., and G.-C. Gong. 2011. Biogeochemical responses in the southern East China Sea after typhoons. *Oceanography* 24(4):42–51, http://dx.doi.org/10.5670/oceanog.2011.93.

Leipper, D., and D. Volgenau. 1972. Hurricane heat potential of the Gulf of Mexico. *Journal of Physical Oceanography* 2:218–224.

Lin, I.-I. In press. Typhoon-induced phytoplankton blooms and primary productivity increase in the western North Pacific subtropical ocean. *Journal of Geophysical Research–Oceans*.

Lin, I.-I., M.-D. Chou, and C.-C. Wu. 2011. The impact of a warm ocean eddy on Typhoon Morakot (2009): A preliminary study from satellite observations and numerical modelling. *Terrestrial Atmospheric and Oceanic Sciences* 22(6), http://dx.doi.org/10.3319/TAO.2011.08.19.01(TM).

Lin, I.-I., W.T. Liu, C.C. Wu, J.C.H. Chiang, and C.H. Sui. 2003a. Satellite observations of modulation of surface winds by typhoon-induced upper ocean cooling. *Geophysical Research Letters* 30, 1131, http://dx.doi.org/10.1029/2002GL015674.

Lin, I.-I., W.T. Liu, C.C. Wu, G.T.F. Wong, C. Hu, Z. Chen, W.D. Liang, Y. Yang, and K.K. Liu. 2003b. New evidence for enhanced ocean primary production triggered by tropical cyclone. *Geophysical Research Letters* 30, 1718, http://dx.doi.org/10.1029/2003GL017141.

Lin, I.-I., C.C. Wu, K.A. Emanuel, I.H. Lee, C.R. Wu, and I.F. Pun. 2005. The interaction of Supertyphoon Maemi (2003) with a warm ocean eddy. *Monthly Weather Review* 133:2,635–2,649, http://dx.doi.org/10.1175/MWR3005.1.

Lin, I.-I., C.C. Wu, I.F. Pun, and D.S. Ko. 2008. Upper ocean thermal structure and the western North Pacific category-5 typhoons: Part I. Ocean features and category-5 typhoon's intensification. *Monthly Weather Review* 136:3,288–3,306, http://dx.doi.org/10.1175/2008MWR2277.1.

Lin, I.-I., C.H. Chen, I.F. Pun, W.T. Liu, and C.C. Wu. 2009a. Warm ocean anomaly, air sea fluxes, and the rapid intensification of tropical cyclone Nargis (2008). *Geophysical Research Letters* 36, L03817, http://dx.doi.org/10.1029/2008GL035815.

Lin, I.-I., I.F. Pun, and C.C. Wu. 2009b. Upper ocean thermal structure and the western North Pacific category-5 typhoons: Part II. Dependence on translation speed. *Monthly Weather Review* 137:3,744–3,757, http://dx.doi.org/10.1175/2009MWR2713.1.

Price, J.F. 1981. Upper ocean response to a hurricane. *Journal of Physical Oceanography* 11:153–175.

Price, J.F. 2009. Metrics of hurricane-ocean interaction: Vertically-integrated or vertically-averaged ocean temperature? *Ocean Science* 5:351–368, http://dx.doi.org/10.5194/os-5-351-2009.

Price, J.F., J. Morzel, and P.P. Niiler. 2008. Warming of SST in the cool wake of a moving hurricane. *Journal of Geophysical Research* 113, C07010, http://dx.doi.org/10.1029/2007JC004393.

Pun, I.F., I.I. Lin, C.R. Wu, D.S. Ko, and W.T. Liu. 2007. Validation and application of altimetry-derived upper ocean thermal structure in the western North Pacific Ocean for typhoon intensity forecast. *IEEE Transactions on Geoscience and Remote Sensing* 45(6):1,616–1,630, http://dx.doi.org/10.1109/TGRS.2007.895950.

Scharroo, R., W.H.F. Smith, and J.L. Lillibridge. 2005. Satellite altimetry and the intensification of Hurricane Katrina. *Eos, Transactions, American Geophysical Union* 86:366–367, http://dx.doi.org/10.1029/2005EO400004

Shay, L.K., G.J. Goni, and P.G. Black. 2000. Effects of a warm oceanic feature on Hurricane Opal. *Monthly Weather Review* 128:1,366–1,383, http://dx.doi.org/10.1175/1520-0493(2000)128<1366:EOAWOF>2.0.CO;2.

Shiah, F.K., S.Y. Chung, S.J. Kao, G.C. Gong, and K.K. Liu. 2000. Biological and hydrographical responses to tropical cyclones (typhoons) in the continental shelf of the Taiwan Strait. *Continental Shelf Research* 20:2,029–2,044, http://dx.doi.org/10.1016/S0278-4343(00)00055-8.

Tsai, Y.L., C.S. Chern, and J. Wang. 2008. Typhoon induced upper ocean cooling off northeastern Taiwan. *Geophysical Research Letters* 35(14), L14605, http://dx.doi.org/10.1029/2008GL034368.

Tseng, Y.H., S. Jan, D.E. Dietrich, I.I. Lin, Y.T. Chang, and T.Y. Tang. 2010. Modeled oceanic response and sea surface cooling to typhoon Kai-Tak. *Terrestrial, Atmospheric and Oceanic Sciences* 21:85–98, http://dx.doi.org/10.3319/TAO.2009.06.08.02(IWNOP).

Webster, P.J., G.J. Holland, J.A. Curry, and H.R. Chang. 2005. Changes in tropical cyclone number, duration and intensity in a warming environment. *Science* 309:1,844–1,846, http://dx.doi.org/10.1126/science.1116448.

Wentz, F.J., C. Gentemann, D. Smith, and D. Chelton. 2000. Satellite measurements of sea surface temperature through clouds. *Science* 288(5467): 847–850, http://dx.doi.org/10.1126/science.288.5467.847.

Wu, C.-R., Y.-L. Chang, L.-Y. Oey, C.-W.J. Chang, and Y.-C. Hsin. 2008. Air-sea interaction between Tropical Cyclone Nari and Kuroshio. *Geophysical Research Letters* 35, L12605, http://dx.doi.org/10.1029/2008GL033942.

Wu, C.C., C.Y. Lee, and I.-I. Lin. 2007. The effect of the ocean eddy on tropical cyclone intensity. *Journal of the Atmospheric Sciences* 64:3,562–3,578, http://dx.doi.org/10.1175/JAS4051.1.

Wu, C.-C., P.-H. Lin, S. Aberson, T.-C. Yeh, W.-P. Huang, K.-H. Chou, J.-S. Hong, G.-C. Lu, C.-T. Fong, K.-C. Hsu, and others. 2005. Dropwindsonde observations for typhoon surveillance near the Taiwan region (DOTSTAR): An overview. *Bulletin of the American Meteorological Society* 86:787–790, http://dx.doi.org/10.1175/BAMS-86-6-787.

Zheng, Z.-W., C.-R. Ho, and N.-J. Kuo. 2008. Importance of pre-existing oceanic conditions to upper ocean response induced by Super Typhoon Hai-Tang. *Geophysical Research Letters* 35, L20603, http://dx.doi.org/10.1029/2008GL035524.